ACS OMEGA

Open Access

http://pubs.acs.org/journal/acsodf

Article

Cooperative Molecular Interaction-Based Highly Efficient Capturing of Ultrashort- and Short-Chain Emerging Per- and Polyfluoroalkyl Substances Using Multifunctional Nanoadsorbents

Avijit Pramanik, Olorunsola Praise Kolawole, Sanchita Kundu, Kaelin Gates, Shivangee Rai, Manoj K. Shukla, and Paresh Chandra Ray*

Cite This: *ACS Omega* 2024, 9, 49452−49462

Read Online

ACCESS | Metrics & More | Article Recommendations | Supporting Information

ABSTRACT: The short-chain (C_4 to C_7) and ultrashort-chain (C_3 to C_2) per- and polyfluoroalkyl substances (PFAS) are bioaccumulative, carcinogenic to humans, and harder to remove using current technologies, which are often detected in drinking and environmental water samples. Herein, we report the development of nonafluorobutanesulfonyl (NFBS) and polyethylene-imine (PEI)-conjugated Fe_3O_4 magnetic nanoparticle-based magnetic nanoadsorbents and demonstrated that the novel adsorbent has the capability for highly efficient removal of six different short- and ultrashort-chain PFAS from drinking and environmental water samples. Reported experimental data indicates that by capitalizing the cooperative hydrophobic, fluorophilic, and electrostatic interaction processes, NFBS-PEI-conjugated magnetic nanoadsorbents can remove ∼100% short-chain perfluorobutanesulfonic acid within 30 min from the water sample with a maximum absorption capacity q_m of ∼234 mg g^{-1}. Furthermore, to show how cooperative interactions are necessary for effective capturing of ultrashort and short PFAS, a comparative study has been performed using PEI-attached magnetic nanoadsorbents without NFBS and acid-functionalized magnetic nanoadsorbents without PEI and NFBS. Reported data show that the ultrashort-chain perfluoropropanesulfonic acid capture efficiency is the highest for the NFBS-PEI-attached nanoadsorbent (q_m ∼ 187 mg g^{-1}) in comparison to the PEI-attached nanoadsorbent (q_m ∼ 119 mg g^{-1}) or carboxylic acid-attached nanoadsorbent (q_m ∼ 52 mg g^{-1}). In addition, the role of cooperative molecular interactions in highly efficient removal of ultrashort-chain PFAS has been analyzed in detail. Moreover, reported data demonstrate that nanoadsorbents can be used for effective removal of short-chain PFAS (<92%) and ultrashort-chain PFAS (<70%) simultaneously from reservoir, lake, tape, and river water samples within 30 min, which shows the potential of nanoadsorbents for real-life PFAS remediation.

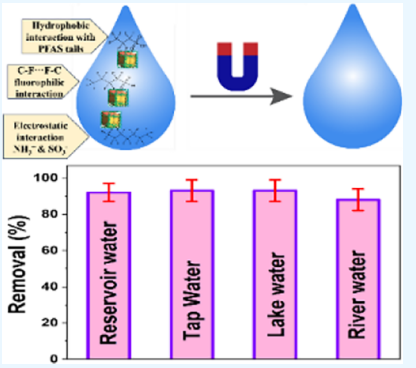

INTRODUCTION

Since 1940, per- and polyfluoroalkyl substances (PFAS) have been used widely in consumer products.[1−10] These manmade "forever chemicals" exhibit resistance to degradation, give rise to adverse health effects, and are bioaccumulative, and thus, the United States Environmental Protection Agency (EPA) have identified them as persistent organic pollutants.[1−10] Since legacy PFAS (C_7 and above) can be responsible for adverse health effects, from 2016, they have been replaced by short-chain and ultrashort-chain PFAS.[1−10]

In the past one decade, industries have used short-chain PFAS like perfluorohexanesulfonate (PFHxS), hexafluoropropylene oxide-dimer acid (GenX), perfluorobutanesulfonic acid (PFBS), and perfluorobutanoic acid (PFBA) and ultrashort-chain PFAS like perfluoropropanesulfonic acid (PFPrS) and trifluoroacetic acid (TFA). As a result, they have been detected in environmental water samples routinely, as well as from human blood, breast milk, and urine.[2−10] In the past few years, several reports detailing toxicity data show that short-chain PFAS are as toxic as legacy PFAS and they can be responsible for kidney failure, cancer, etc.[1−10] It is also well documented that short-chain PFAS are harder to remove from contaminated water due to their higher mobility and hydrophilicity,.[11−20] To tackle the ultrashort- and short-chain PFAS contamination in water, this work reports the development of nonafluorobutanesulfonyl (NFBS) and polyethylenimine (PEI)-conjugated Fe_3O_4 magnetic nanoparticle-based nanoadsorbents that have the capability for highly efficient removal of short-chain PFAS like GenX, PFHxS, PFBS, and PFBA and ultrashort-chain PFAS like PFPrS and TFA from water samples by leveraging cooperative fluorophilicity and electrostatic interactions.

Received: August 4, 2024
Revised: November 13, 2024
Accepted: November 19, 2024
Published: December 8, 2024

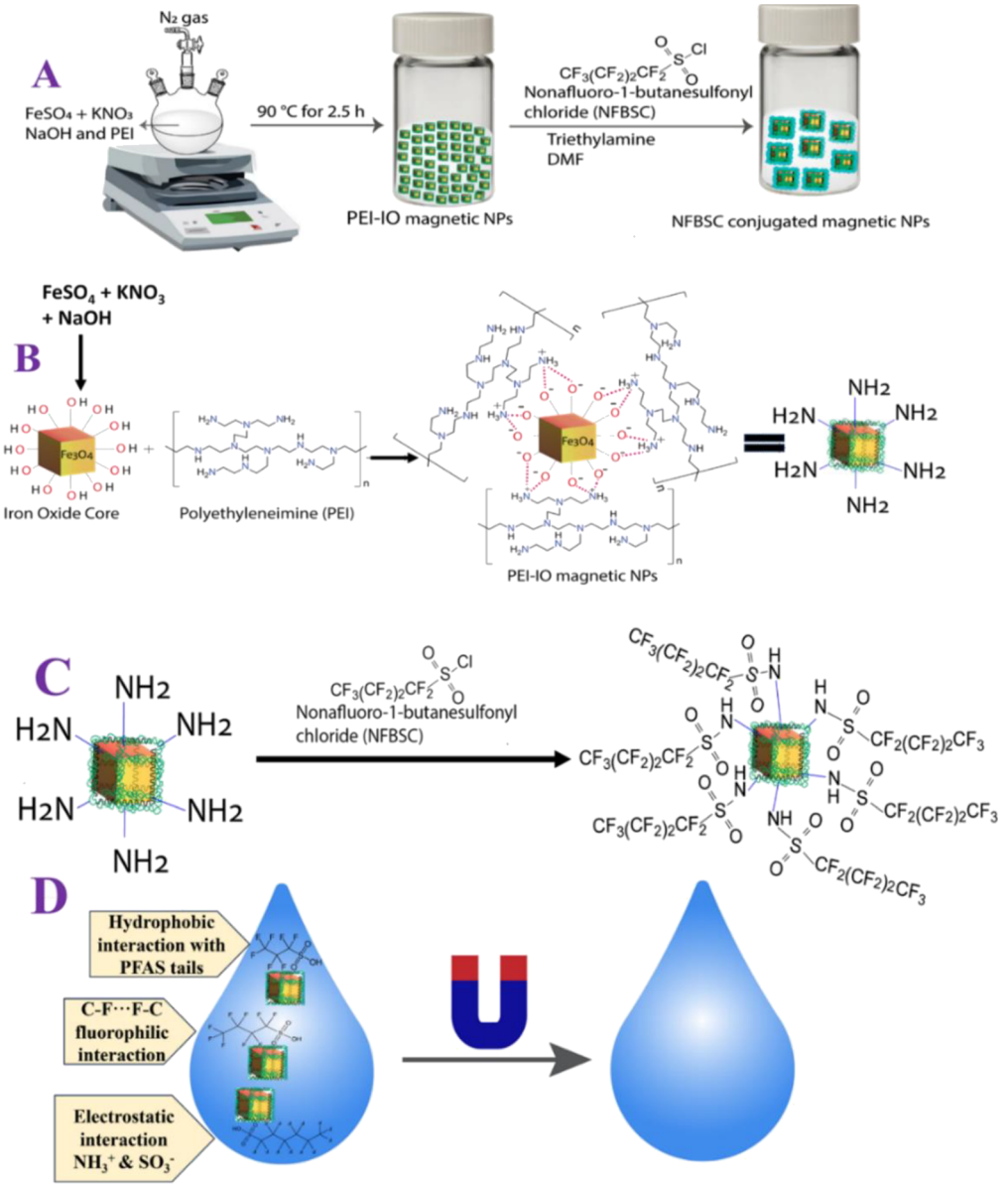

Figure 1. (A–C) Scheme showing the synthetic process that we have used for the development of nonafluoro-butanesulfonyl (NFBS) and polyethylene imine (PEI)-conjugated Fe_3O_4 magnetic nanoparticle-based multifunctional magnetic nanoadsorbents. (D) Scheme showing the use of magnetic nanoadsorbents for the separation of short-chain and ultrashort-chain PFAS from water.

Since adsorption is a versatile method to capture and remove PFAS from water, scientists have designed novel adsorbents such as activated carbon, ionic fluorogel, calixarene, fluorinated graphene oxide, and electrospun nanofibrous-based adsorbents for PFAS removal.[16−34] PFAS can be removed by different adsorbents using dipole−dipole, electrostatic, ionic−dipolar, hydrophilic, and fluorophilic interactions.[10−25] However, recent reports show that the removal efficiency is much lower for ultrashort- and short-chain PFAS in comparison to that for legacy PFAS.[22−34] To improve the removal efficiency, we have designed NFBS and PEI-conjugated magnetic nanoadsorbents for high affinity removal of ultrashort- and short-chain PFAS like GenX, PFHxS, PFBS, PFBA, TFA, and PFPrS using a combination of hydrophobic, fluorophilic, and electrostatic interactions. To determine the role of electrostatic, ionic−dipolar, hydrophobic, and fluorophilic interactions in capturing and removal of ultrashort- and short-chain PFAS, we have performed the same experiment with a PEI-attached Fe_3O_4 magnetic nanoparticle-based nanoadsorbent, a F-PEG-COOH-attached Fe_3O_4 magnetic nanoparticle-based nanoadsorbent, and a carboxy-attached Fe_3O_4-magnetic nanoparticles. The reported data show that the maximum removal efficiency is observed for NFBS and PEI-conjugated magnetic nanoadsorbents, which is due to the presence of cooperative hydrophobic and fluorophilic interactions and an electrostatic attraction mechanism.

MATERIALS AND METHODS

Synthesis of PEI-Attached Fe_3O_4 Nanoparticles. Amine-functionalized cubic-shaped iron oxide magnetic nanoparticles were synthesized using a previously reported procedure.[35−39] Experimental details are reported in the Supporting Information. In brief, as shown in Figure 1A,B, 0.35 g [1 mM] of ferrous sulfate heptahydrate ($FeSO_4·7H_2O$), 5 mL of 2.0 M potassium nitrate (KNO_3), and 5.0 mL of 1.0 M

https://doi.org/10.1021/acsomega.4c07159
ACS Omega 2024, 9, 49452−49462

sodium hydroxide (NaOH) were mixed in 100 mL of double distilled water under a nitrogen atmosphere. After that, 10 mL (0.32 mM) of polyethylenimine (PEI, branched, MW ∼ 25 000) was added to the reaction mixture and then heated at 90 °C for another 2.5 h under a nitrogen atmosphere. The solution color turned from blue to black, indicating the formation of PEI-branched iron oxide magnetic nanoparticles. Then, the black precipitate obtained was thoroughly washed with distilled water and magnetically separated by a neodymium disk magnet. To remove the excess reactants, magnetic separation and redispersion in ultrapure water were performed repeatedly. Finally, the solid powder was obtained by drying it under vacuum for a few days.

Synthesis of NFBS and PEI-Conjugated Multifunctional Magnetic Nanoadsorbents. For the synthesis of nonafluorobutanesulfonyl and PEI-conjugated Fe_3O_4 magnetic nanoparticle-based nanoadsorbents (shown in Figure 1A−C), 50 mg of the PEI-functionalized Fe_3O_4 powder magnetic nanoparticles were added to 10 mL (6.8 mM) of dry DMF solution and then were sonicated for a minute. Then, 2 mL of triethyl amine (99.5%) was then added to the dispersed magnetic nanoparticle solution. Then, the nanoadsorbents were thoroughly washed with distilled water and magnetically separated with a neodymium disk magnet. To remove the excess reactants and other reaction products like HCl, magnetic separation and redispersion in ultrapure water were performed repeatedly. Finally, the dried solid nanoadsorbents were collected under reduced pressure at room temperature.

Removal Efficiency and Capturing Kinetics for Ultrashort- and Short-Chain PFAS Using NFBS and PEI-Conjugated Multifunctional Magnetic Nanoadsorbents. For the determination of the removal amount for short- and ultrashort-chain PFAS like GenX, PFHxS, PFBS, and PFPrS using NFBS and PEI-conjugated multifunctional magnetic nanoadsorbents, PFAS and nanoadsorbents were stirred for different times.[10−20] Figure S1B in the Supporting Information shows the schematic representation of the experimental setup and procedure that we used to determine the removal efficiency and capturing kinetics. As shown in Figure S1B, initially adsorbed PFAS with nanoadsorbents were separated magnetically using neodymium disk magnets. To determine the time-dependent separation efficiency and kinetics, a 1 mL aliquot was taken at each predetermined time intervals. After that, the aliquots were centrifuged for 15 min, as shown in Figure S1B. In the next step, as shown in Figure S1B, the supernatant was analyzed using LC-MS to determine the residual GenX, PFHxS, PFBS, and PFPrS concentration. For this purpose, we have used LC-MS (Agilent Technologies)[10−20] and the X Bridge-C18 column (4.6 mm × 250 mm) from Agilent Technologies.[10−20] For the analysis, we have used negative ionization (ESI−) mode.[10−20] For the processing the data, we have used the MassLynx workstation.[10−20] We have also performed control experiments to account for the losses of GenX, PFHxS, PFBS, and PFPrS during handling. For this purpose, we performed experiments under identical conditions, where NFBS and PEI-conjugated multifunctional magnetic nanoadsorbents are absent. The removal efficiency for short-chain and ultrashort-chain PFAS like GenX, PFHxS, PFBS, and PFPrS was determined using eq 1:[10−20]

$$\text{PFAS removal efficiency}(\%) = \frac{C_I - C_t}{C_i} \times 100 \quad (1)$$

where C_I is the concentration of short- and ultrashort-chain PFAS before separation and C_t is the concentration of short- and ultrashort-chain PFAS at time t during the separation process.

The adsorbed PFAS amounts were determined using the mass difference between the blank controls, which have been performed without an adsorbent and test groups in the presence of adsorbents with the same contact time, divided by the mass of the added adsorbent.[10−20] The amounts of absorbed short- and ultrashort-chain PFAS by NFBS and PEI-conjugated magnetic nanoadsorbents were determined using eq 2, as we and others have reported before:[10−20]

$$q_t = \frac{C_I - C_t}{C_A} \quad (2)$$

where q_t is the amount of short- and ultrashort-chain PFAS absorbed separately per gram of NFBS and PEI-conjugated magnetic nanoadsorbents at time t and C_I is the concentration of short- and ultrashort-chain PFAS before separation. Similarly, C_t is the concentration of short- and ultrashort-chain PFAS at time t during the separation process. On the other hand, C_A is the concentration of the NFBS and PEI-conjugated magnetic nanoadsorbents.

We have determined the rate of removal of short- and ultrashort-chain PFAS like GenX, PFHxS, PFBS, PFBA, TFA, and PFPrS via adsorption by NFBS and PEI-conjugated magnetic nanoadsorbents, by using Ho and McKay's pseudo-second-order adsorption model as we and others have reported before.[10−20] For this purpose, we have used eq 3 as shown below:

$$\frac{t}{q_t} = \frac{t}{q_{equ}} + \frac{1}{K_{obs} q_{equ}^{\ 2}} \quad (3)$$

where q_t is the amount of short- and ultrashort-chain PFAS absorbed separately per gram of NFBS and PEI-conjugated magnetic nanoadsorbents at time t. On the other hand, q_{equ} is the quantity of emerging short- and ultrashort-chain PFAS absorbed separately at equilibrium, and k_{obs} is the rate constant for the separation process via adsorption using NFBS and PEI-conjugated magnetic nanoadsorbents. The rate constant k_{obs} can be calculated from the intercept and slope of the plot of t/q_t against t. All the batches of kinetic experiments for the removal of GenX, PFHxS, PFBA, TFA, and PFPrS via adsorption by NFBS and PEI-conjugated magnetic nanoadsorbents were performed in triplicate. For determining the maximum adsorption capacity for each short- and ultrashort-chain PFAS using NFBS and PEI-conjugated magnetic nanoadsorbents, we have used the Langmuir adsorption model as we and others have reported before, shown in eq 4:[10−20]

$$\frac{1}{q_{equ}} = \frac{t}{q_m} + \frac{1}{bC_{equ}q_m} \quad (4)$$

where q_{equ} is the quantity of short- and ultrashort-chain PFAS adsorbed separately at equilibrium, q_m is the maximum capacity of each short- and ultrashort-chain PFAS adsorption by NFBS and PEI-conjugated magnetic nanoadsorbents at equilibrium, C_{equ} is the concentration of each short- and ultrashort-chain PFAS, and b is a Langmuir constant for the adsorption process. The experimental data for the removal of GenX, PFHxS, PFBS, PFBA, TFA, and PFPrS was fitted with

https://doi.org/10.1021/acsomega.4c07159
ACS Omega 2024, 9, 49452−49462

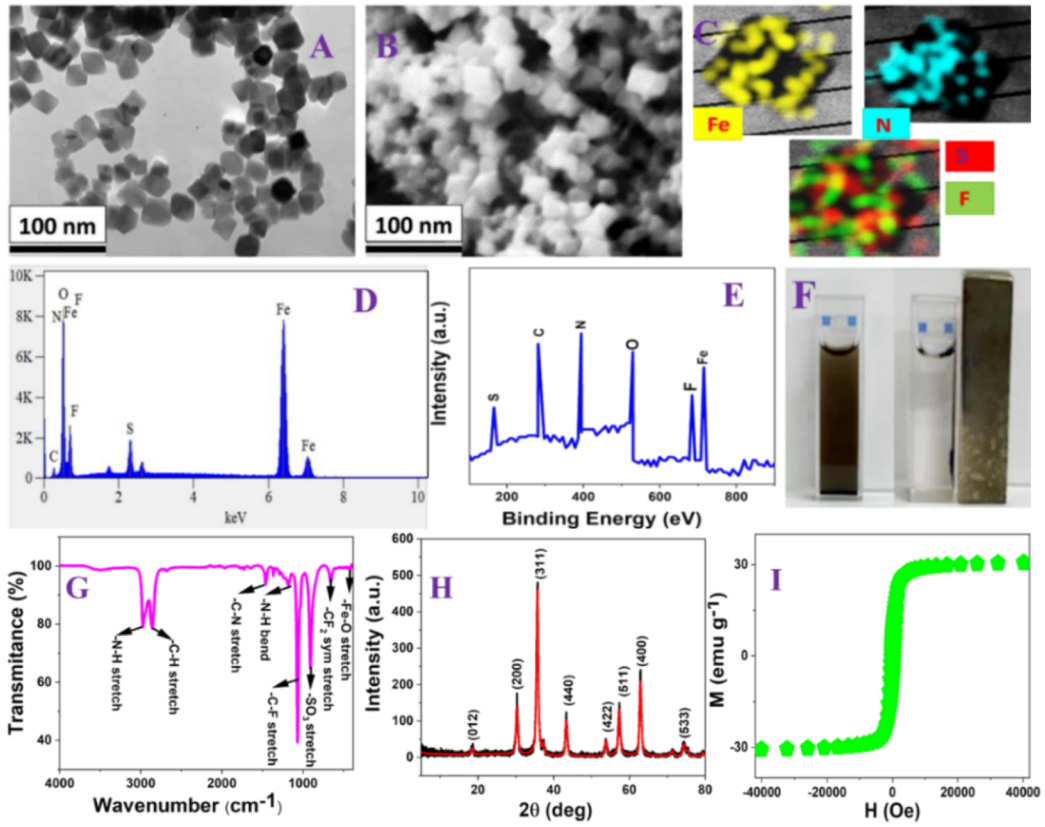

Figure 2. (A) TEM image from PEI-functionalized Fe_3O_4 magnetic nanoparticles. (B) SEM image from NFBS and PEI-conjugated magnetic nanoadsorbents. (C) Energy-dispersive X-ray spectroscopy (EDX) mapping data from nanoadsorbents. (D) EDX analysis showing particle constituents in nanoadsorbents. (E) XPS spectrum from the nanoadsorbent. (F) Picture showing that the nanoadsorbents can be used for the separation of emerging and legacy PFAS from water samples using a small bar magnet. (G) FTIR spectra from the nanoadsorbent. (H) X-ray diffraction (XRD) analysis from the nanoadsorbent. (I) Magnetic curve from the nanoadsorbent.

the Langmuir and Freundlich isotherm models, and q_m was obtained from the intercept and the slope. For this purpose, experiments were performed in triplicate.

RESULTS AND DISCUSSION

Microscopic and Spectroscopic Characterization of NFBS and PEI-Conjugated Multifunctional Magnetic Nanoadsorbents. As we have discussed before, NFBS and PEI-conjugated magnetic nanoadsorbents were designed by using a two-step procedure. Initially, amine-functionalized cubic-shaped iron oxide magnetic nanoparticles were synthesized using $FeSO_4{\cdot}7H_2O$, KNO_3, NaOH, and PEI.[35−39] After purification, we characterized the magnetic nanoparticles using a tunneling electron microscope (TEM).[35−39] As reported in Figure 2A, the PEI-conjugated Fe_3O_4 magnetic nanoparticles can be classified as having the shape of nanocubes, and the size is 30 ± 3 nm. We have also measured the size of PEI-conjugated Fe_3O_4 magnetic nanoparticles using a dynamic light scattering (DLS) technique.[35−39] Figure S2B in the Supporting Information shows the particle size distribution histogram of PEI-attached Fe_3O_4 magnetic nanoparticles, indicating that the size is 30 ± 6 nm, which matches very well with TEM data. The measured zeta potential value for Fe_3O_4 magnetic nanoparticles without PEI was −20.6 mV. On the other hand, the measured zeta potential value for PEI-attached Fe_3O_4 magnetic nanoparticles was +3.93 mV, which indicates that PEI has been attached on the iron oxide nanoparticle surface. As reported in Figure 1B, in PEI-Fe_3O_4 nanoparticles, PEI is attached with iron oxide core nanoparticles via electrostatic interactions. As reported in Figure S3 in the Supporting Information, the FTIR spectra from Fe_2O_3 nanoparticles without PEI show the presence of −OH stretch, −OH bend, and −Fe−O stretch peaks, which indicates that we have designed a hydroxy-conjugated iron oxide core nanoparticle. On the other hand, as reported in Figure S4 in the Supporting Information, the FTIR spectra from PEI-attached Fe_2O_3 nanoparticles show the presence of the −NH stretch, −CH stretch, −NH bend, −CH bend, −CN stretch, −CN bends, and Fe−O stretch peaks, which indicates that PEI are attached to the iron oxide core nanoparticle. As reported in Figure S5 in the Supporting Information, the TGA curve shows the percentage (%) of weight loss during thermal decomposition from Fe_2O_3 nanoparticles without PEI and PEI-attached Fe_2O_3 nanoparticles, which indicates 8% more weight loss for PEI-attached Fe_2O_3 nanoparticles in comparison to Fe_2O_3 nanoparticles without PEI. Using elemental analysis, as reported in Table S1 in the Supporting Information and TGA data, we determined that the weight percentage of PEI is ∼8%. The superparamagnetic property measurement using a SQUID magnetometer[35−39] indicates that the specific saturation magnetization for PEI-conjugated Fe_3O_4 magnetic nanoparticles is ∼31.4 emu g^{-1}. In the second step, NFBS and PEI-conjugated magnetic nanoadsorbents were developed using PEI-coated magnetic nanoparticles, DMF, and triethylamine. The synthesis details are reported in the Supporting

https://doi.org/10.1021/acsomega.4c07159
ACS Omega 2024, 9, 49452−49462

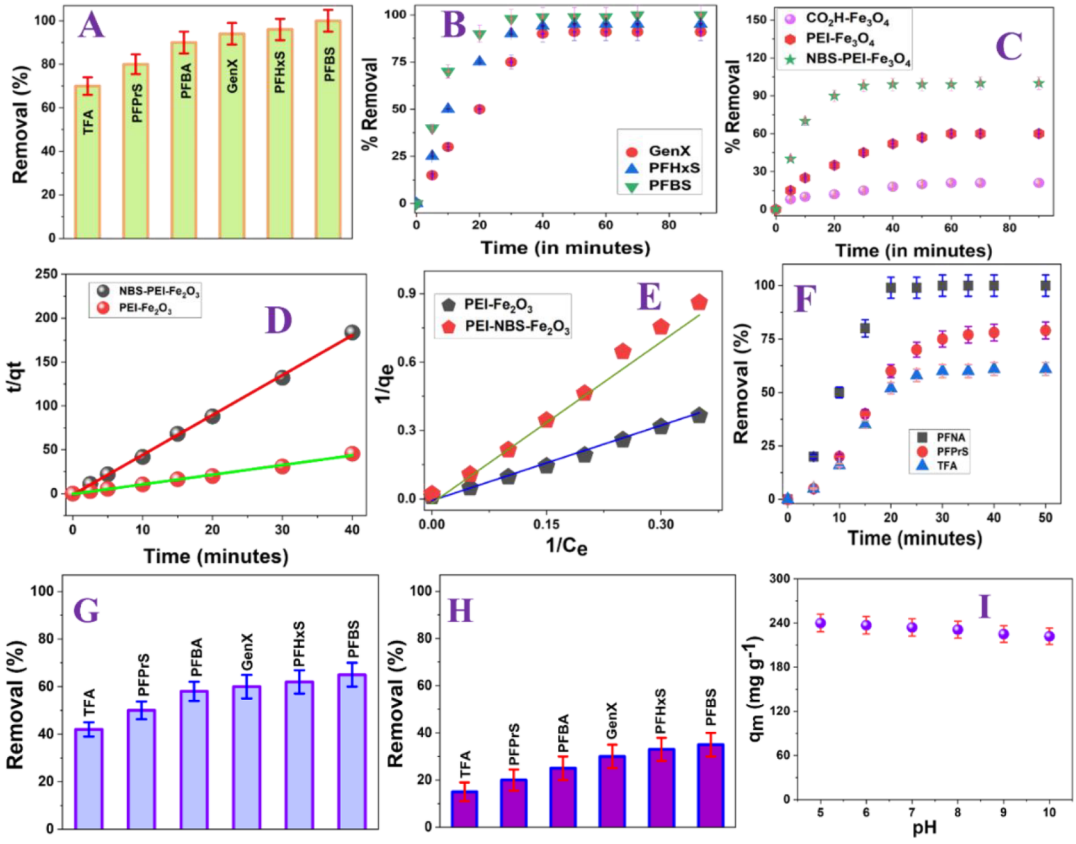

Figure 3. (A) Removal efficiency for short- and ultrashort-chain PFAS (1 μg/L) from drinking water using the NFBS and PEI-attached magnetic nanoadsorbent (1 mg/L). (B) Plot showing the time-dependent removal efficiency for short-chain PFAS using the nanoadsorbent. (C) Plot showing the time-dependent removal efficiency for short-chain PFBS from drinking water using different nanoadsorbents. (D) Plot showing how t/q_t varies with time for PFBS removal from drinking water. (E) Plot showing how $1/q_e$ varies with $1/C_e$ for PFBS removal from drinking water. (F) Plot showing the time-dependent removal efficiency for PFNA, PFPrS, and NFA using the nanoadsorbent. (G) Removal efficiency for short- and ultrashort-chain PFAS (1 μg/L) from drinking water using the PEI-attached magnetic nanoadsorbent (1 mg/L). (H) Removal efficiency for short- and ultrashort-chain PFAS (1 μg/L) from drinking water using the carboxy-attached magnetic nanoadsorbent (1 mg/L). (I) Plot showing pH-dependent PFBS removal efficiency using the nanoadsorbent.

Information. After purification, we characterized the nanoadsorbents using scanning electron microscopy (SEM).[35−39]

As reported in Figure 2B, the NFBS and PEI-conjugated magnetic nanoadsorbent shape is classified as a nanocube, and the size is 35 ± 5 nm. We have also measured the size of NFBS and PEI-conjugated magnetic nanoadsorbents using the DLS technique. Figure S2C in the Supporting Information shows the particle size distribution histogram of PEI and NFBS-attached Fe_3O_4 magnetic nanoparticles, which indicates that the size is 35 ± 6 nm, matching very well with SEM data. The measured zeta potential value for NFBS and PEI-attached Fe_3O_4 magnetic nanoparticles was −1.3 mV. Since the zeta potential value for PEI-attached Fe_3O_4 magnetic nanoparticles was +3.93 mV and the zeta potential value for nanoadsorbents was observed as −1.3 mV, this indicates that NFBS has been attached on the nanoadsorbent surface.

Figure 2C shows the energy-dispersive spectrometry (EDS) mapping data, which clearly show the presence of Fe, F, N, and S. The EDS spectra from nanoadsorbents are reported in Figure 2D and show the presence of Fe, N, C, S, O, and F. Figure 2E reports the X-ray photoelectron spectroscopy (XPS) data from NFBS and PEI-conjugated magnetic nanoadsorbents, confirming peaks at 166.2, 288.5, 401.6, 533.2, 688.3, and 710.6 eV that are due to S, C, N, O, F, and Fe, respectively.[35−39] The X-ray diffraction (XRD) data reported in Figure 2H for NFBS and PEI-conjugated magnetic nanoadsorbents shows the presence of (012), (200), (311), (440), (422), (511), (400), and (533) indices, which indicate that the magnetic nanoparticle is in the hematite phase.[35−39]

Figure 2G shows the FTIR spectra from NFBS and PEI-conjugated magnetic nanoadsorbents. These spectra indicate the presence of Fe−O stretch, $-CF_2$ symmetric stretch, −C−F stretch, $-SO_3$ stretch, −C=O, −N−H bend, −N−H stretch, −C−N stretch, and −C−H stretch peaks,[35−39] which indicates that both PEI and NFBS are present on the iron oxide core nanoparticle. As reported in Figure S5 in the Supporting Information, the TGA curve shows the percentage (%) of weight loss during thermal decomposition from Fe_2O_3 nanoparticles without PEI, PEI-attached Fe_2O_3 nanoparticles, and NFBS-PEI-attached Fe_2O_3 nanoparticles, which indicate 6% more weight loss for NFBS and PEI-attached Fe_2O_3 nanoparticles in comparison to only PEI-attached Fe_2O_3 nanoparticles. Figure 2I shows the magnetic curve from NFBS and PEI-conjugated magnetic nanoadsorbents and shows that the specific saturation magnetization is ∼28.9 emu g^{-1}. The graph in Figure 2F shows that NFBS and PEI-conjugated magnetic nanoadsorbents can be used for the separation of emerging and legacy PFAS from water samples using a small bar magnet.

https://doi.org/10.1021/acsomega.4c07159
ACS Omega 2024, 9, 49452−49462

Capturing Short-Chain PFAS like GenX, PFHxS, PFBS, and PFPrS from Drinking Water Using NFBS and PEI-Conjugated Magnetic Nanoadsorbents. We have performed flowing experiments to determine the capture and separation efficiency of ultrashort- and short-chain PFAS like GenX, PFHxS, PFBS, PFBA, TFA, and PFPrS from drinking water using NFBS and PEI-conjugated magnetic nanoadsorbents. Initially, the drinking water sample was spiked with ultrashort- and short-chain PFAS like GenX, PFHxS, PFBS, PFBA, TFA, and PFPrS individually and simultaneously. To understand selective emerging PFAS separation, drinking water samples were spiked with 1 μg/L GenX, PFHxS, PFBS, PFBA, TFA, and PFPrS individually. To determine the separation ability in a mixture of shorter-chain PFAS, the drinking water sample was spiked with 0.33 μg/L GenX, PFHxS, PFBS, PFBA, TFA, and PFPrS simultaneously. After that, the capturing and removal efficiency was determined using LC-MS (see the Supporting Information for details). Our nanoarchitectures have a fair amount of F present. To understand whether the nanoadsorbents are stable in water at different pH levels, the NFBS and PEI-conjugated magnetic nanoadsorbents were exposed to water for a few weeks and the amount of F released was measured using LC-MS.[10−20] No F was released from nanoadsorbents even after being exposed to water for 1 month at pH 7. We have also performed structural analysis using XRD, FTIR spectroscopy, and XPS before and after exposure to water, which indicates that the structure remains very similar. Since no F was released and the NFBS-conjugated magnetic nanoarchitecture can be removed from water by a magnet, we can use this design of nanoarchitecture very safely for the removal of PFAS.

As reported in Figure 3A, the capture and removal efficiency for emerging short-chain PFBS is ∼100% when the NFBS and PEI-conjugated magnetic nanoadsorbent has been used. Similarly, the capturing and removal efficiency for short-chain PFHxS is ∼94% when the NFBS and PEI-conjugated magnetic nanoadsorbent has been used. In addition, the capturing and removal efficiency for short-chain GenX is ∼92% and that for PFBS is ∼88% when the NFBS and PEI-conjugated magnetic nanoadsorbent has been used.

On the other hand, the capturing and removal efficiency for ultrashort-chain PFPrS is ∼80% and that for TFA is ∼71% when the NFBS and PEI-conjugated magnetic nanoadsorbent has been used.

Finding the Kinetics for the Emerging PFAS Capturing Process Using NFBS and PEI-Conjugated Multifunctional Magnetic Nanoadsorbents. Figure 3B shows the time-dependent removal efficiency for shorter-chain PFAS such as PFBS, PFHxS, and GenX from drinking water using the NFBS and PEI-conjugated magnetic nanoadsorbent. Reported kinetics data show that the emerging PFBS removal efficiency reached ∼100% within 30 min when the nanoadsorbent has been used as an adsorber. As reported in Figure 3B, the PFBS removal efficiency remains the same after 30 min.

On the other hand, as shown in Figure 3B, the removal efficiency for GenX reached ∼75% after 30 min and 92% after 40 min. Next, we have determined the rate of removal of emerging PFAS like GenX, PFHxS, and PFBS via adsorption by the NFBS and PEI-conjugated magnetic nanoadsorbent, as reported in Figure 3C−E. For this purpose, we have used Ho and McKay's pseudo-second-order adsorption model,[10−20] as we have discussed in the Materials and Methods Section and reported in eq 3. Using experimental data and eq 3, we have estimated that the maximum capacity of PFBS adsorption by the NFBS and PEI-conjugated magnetic nanoadsorbent at equilibrium (q_m) is ∼234 mg g^{-1}. Similarly, the estimated maximum capacity of GenX adsorption by NFBS and PEI-conjugated magnetic nanoadsorbents at equilibrium (q_m) is ∼219 mg g^{-1}. As shown in Table 1, the experimentally observed maximum GenX adsorption capacity by the NFBS and PEI-conjugated magnetic nanoadsorbent is comparable with the magnetic fluorinated polymer-based adsorbent reported by Tan et al. (q_m = 219 mg g^{-1} for GenX),[17] β-CD polymer-based adsorbent by Yang et al. (q_m = 222 mg g^{-1} for GenX),[29] and ionic fluorogel-based adsorbent reported by Kumarasamy et al. (q_m = 217 mg g^{-1} for GenX).[13] The experimentally observed maximum PFHxS adsorption capacity by the NFBS and PEI-conjugated magnetic nanoadsorbent at equilibrium (q_m) is ∼226 mg g^{-1}. The reported q_m value is much higher than the literature reported value for the magnetic (Fe_3O_4) PAC-based adsorbent.[31] Figure 3F shows the time-dependent removal efficiency for ultrashort-chain PFAS such as TFA and PFPrS from drinking water using the NFBS and PEI-conjugated magnetic nanoadsorbent. Using time-dependent data and eq 3, we estimated that the maximum capacity of TFA adsorption by NFBS and PEI-conjugated magnetic nanoadsorbents at equilibrium (q_m) is ∼170 mg g^{-1}. Similarly, using time-dependent data and eq 3, we have estimated that the maximum capacity of PFPrS adsorption by NFBS and PEI-conjugated magnetic nanoadsorbents at equilibrium (q_m) is ∼186 mg g^{-1}. As shown in Table 1, the experimentally observed maximum TFA adsorption capacity by the NFBS and PEI-conjugated magnetic nanoadsorbent is comparable with the zirconium MOF adsorbent reported by Zhang et al. (q_m = 193 mg g^{-1} for TFA).[21]

Table 1. Comparison of the Adsorption Capacity (q_m) Observed Using the NFBS and PEI-Conjugated Multifunctional Magnetic Nanoadsorbent and Different Sorbents Reported in the Literature

system	PFAS	q_m	ref
NFBS-PEI-Fe_2O_3	PFNA	246 mg g^{-1}	this work
NFBS-PEI-Fe_2O_3	PFBS	234 mg g^{-1}	this work
NFBS-PEI-Fe_2O_3	PFHxS	226 mg g^{-1}	this work
NFBS-PEI-Fe_2O_3	GenX	219 mg g^{-1}	this work
NFBS-PEI-Fe_2O_3	PFBA	202 mg g^{-1}	this work
NFBS-PEI-Fe_2O_3	PFPrS	186 mg g^{-1}	this work
NFBS-PEI-Fe_2O_3	TFA	170 mg g^{-1}	this work
magnetic fluorinated polymer	GenX	219 mg g^{-1}	17
magnetic (Fe_3O_4) PAC	PFHxS	132 mg g^{-1}	31
ionic fluorogels	GenX	217 mg g^{-1}	13
2D COF	GenX	200 mg g^{-1}	26
β-CD polymer	GenX	222 mg g^{-1}	29
PEI-FGO	PFNA	208 mg g^{-1}	20
zirconium MOF	PFBA	274 mg g^{-1}	21
zirconium MOF	TFA	193 mg g^{-1}	21

Understanding the Role of Noncovalent Hydrophobic, Fluorophilic, and Electrostatic Interactions in Effective Capturing of Short-Chain PFAS. As reported in Figure 3A,B, using the NFBS and PEI-conjugated magnetic nanoadsorbent, the separation efficiency for PFBS is the highest in comparison with other emerging short-chain PFAS that we have used. In perfluorobutanesulfonic acid (PFBS), the

https://doi.org/10.1021/acsomega.4c07159
ACS Omega 2024, 9, 49452−49462

C−F groups are hydrophobic as well as highly dipolar.[10−20] As a result, PFBS can participate in electrostatic, hydrophobic, and fluorophilic interactions with the NFBS and PEI-conjugated magnetic nanoadsorbent.[10−20] The hydrophobic interaction is the molecular London's dispersion force interactions between the alkyl chain in PFBS and NFBS-PEI conjugated adsorbents.[10−20] Due to the long alkyl chain, hydrophobic interaction can be a strong adsorption mechanism for PFBS capturing using the NFBS and PEI-conjugated magnetic nanoadsorbent.[10−20] The fluorophilic interactions, which arise due to the C−F···F−C interaction between PFBS and nanoadsorbents, are known to be a promising force to provide strong adsorption capacity[20−34] to the strong electronegativity of F in nanoadsorbents; the material has a strong capability to polarize nearby atoms, which provide specific fluorous interactions with PFBS.[10−20] As a result, fluorous interactions can be the prominent adsorption mechanism for PFBS capturing using magnetic nanoadsorbents.[10−20] On the other hand, PFBS has a hydrophilic head and a fluorophilic tail. Since the pK_a for PFBS is ∼−3.3, PFBS exists in mostly ionic form at pH 7.[10−20] Due to the ionic nature of PFBS, the electrostatic interactions between the amine group of the magnetic nanoadsorbent and PFBS are strong.[10−20] As a result, these electrostatic interactions can be a prominent adsorption mechanism for PFBS capture using a magnetic nanoadsorbent. By capitalizing on the cooperative hydrophobic, fluorophilic, and electrostatic interaction processes, NFBS-PEI-conjugated Fe_3O_4 magnetic nanoadsorbents are capable for ∼100% PFBS removal within 30 min. Similarly, as reported in Figure 3F, using cooperative hydrophobic, fluorophilic, and electrostatic interaction processes, NFBS-PEI-conjugated Fe_3O_4 magnetic nanoadsorbents are capable of ∼100% PFNA removal within 22 min. Moreover, as reported in Figure 3B, cooperative hydrophobic, fluorophilic, and electrostatic interaction processes help to capture 98% PFHxS using NFBS-PEI-conjugated Fe_3O_4 magnetic nanoadsorbents.

Next, to understand the role of cooperative hydrophobic, fluorophilic, and electrostatic interaction in capture and removal of emerging PFBS, we have performed the same experiment with the PEI-conjugated magnetic nanoadsorbent and carboxy-conjugated magnetic nanoparticle. Figure 3G shows the removal efficiency for short- and ultrashort-chain PFAS from drinking water using a PEI-attached magnetic nanoadsorbent. Similarly, Figure 3H shows the removal efficiency for short- and ultrashort-chain PFAS from drinking water using the F-PEG-COOH-attached magnetic nanoadsorbent. Figure 3C shows the time-dependent removal efficiency for short-chain PFBS from drinking water using the NFBS and the PEI-conjugated magnetic nanoadsorbent. Figure 3C also shows the time-dependent removal efficiency for short-chain PFBS from drinking water using the PEI-conjugated magnetic nanoadsorbent and carboxy-conjugated magnetic nanoparticle. Reported kinetics data show that the emerging PFBS removal efficiency reached ∼100% within 30 min when the NFBS and PEI-conjugated magnetic nanoadsorbent has been used. As reported in Figure 3C, the PFBS removal efficiency reaches ∼60% after 80 min when the PEI-conjugated magnetic nanoadsorbent without NFBS has been used. Similarly, as shown in Figure 3C, the removal efficiency for PFBS reached ∼20% after 90 min when the acid-functionalized magnetic nanoadsorbent without PEI and NFBS was used. Similarly, as reported in Figure 3B, PFH_XS removal efficiency reached ∼98% within 30 min when the NFBS and PEI-conjugated magnetic nanoadsorbent has been used. On the other hand, as reported in Figure 3G, the PFH_XS removal efficiency reached ∼56% after 80 min when the PEI-conjugated magnetic nanoadsorbent without NFBS was used. Moreover, as shown in Figure 3H, the removal efficiency for PFBS reached ∼18% after 90 min when the acid-functionalized magnetic nanoadsorbent without PEI and NFBS was used.

Using experimental data reported in Figure 3C−E and eq 3, we have estimated the maximum capacity of PFBS adsorption by different magnetic nanoadsorbents, which shows that perfluorobutanesulfonic acid (PFBS) capturing efficiency is the highest for the NFBS-PEI-attached magnetic nanoadsorbent (q_m ∼ 234 mg g^{-1}), in comparison to the PEI-attached magnetic nanoadsorbent (q_m ∼ 139 mg g^{-1}) or carboxylic acid-attached magnetic nanoadsorbent without NFBS and PEI (q_m ∼ 89 mg g^{-1}). Similarly, we have estimated the maximum capacity (q_m) of PFH_XS adsorption for the NFBS-PEI-attached magnetic nanoadsorbent (∼226 mg g^{-1}), which is much higher than those of the PEI-attached magnetic nanoadsorbent (q_m ∼ 127 mg g^{-1}) or carboxylic acid-attached magnetic nanoadsorbent without NFBS and PEI (q_m ∼ 72 mg g^{-1}). Moreover, we have estimated the maximum capacity (q_m) of PFPrS adsorption for the NFBS-PEI-attached magnetic nanoadsorbent as ∼186 mg g^{-1}, which is much higher than those of the PEI-attached magnetic nanoadsorbent (q_m ∼ 93 mg g^{-1}) or carboxylic acid-attached magnetic nanoadsorbent without NFBS and PEI (q_m ∼ 47 mg g^{-1}). All the above data clearly indicates that the separation efficiency and kinetics of separation are the highest for the NFBS and PEI-conjugated magnetic nanoadsorbent. The factors leading to a better separation efficiency for the NFBS and PEI-conjugated magnetic nanoadsorbent are detailed below.

In the case of acid-functionalized magnetic nanoadsorbents, PFBS can interact with the nanoadsorbent mainly via hydrophobic interactions. Now, due to the presence of $-CO_2H$, the sorbent carries a negative surface charge. Since the pK_a for PFBS is ∼−3.3,[10−20] PFBS exists mostly in ionic form at pH 7, and as a result, the interaction between the adsorbent and PFBS will be a repulsive electrostatic interaction. Repulsive interactions lead to a low removal efficiency when an acid-functionalized magnetic nanoadsorbent without NFBS and PEI has been used. However, in the case of the PEI-conjugated magnetic nanoadsorbent, the presence of a unique −N−H bond from PEI allows the nanoadsorbent to interact with PFBS using hydrophobic and electrostatic interactions. As we have discussed before, since the pK_a for PFBS is ∼−3.3,[10−20] PFBS exists in mostly its ionic form, and as a result, it can undergo strong electrostatic interactions with the cationic amines of the PEI. These electrostatic interactions play a very important role in enhancing the removal efficiency.[10−20] As a result (Figure 3C), experimental data show a 60% PFBS removal capability for the PEI-conjugated magnetic nanoadsorbent. On the other hand (Figure 3C), we have observed ∼99% separation of PFBS when the NFBS and PEI-conjugated magnetic nanoadsorbent have been used. In this case, the presence of unique C−F bonds from NFBS and −N−H bonds from PEI allows the nanoadsorbent to interact with PFBS using hydrophobic, electrostatic, and fluorophilic interactions, which leads to an excellent removal capacity.

Next, to determine how the PFBS removal efficiency varies in the absence of PEI, we have designed a magnetic nanoadsorbent using F-PEG-CH_2COOH [poly(ethylene glycol)], containing fluorine and carboxylic acid.

https://doi.org/10.1021/acsomega.4c07159
ACS Omega 2024, 9, 49452−49462

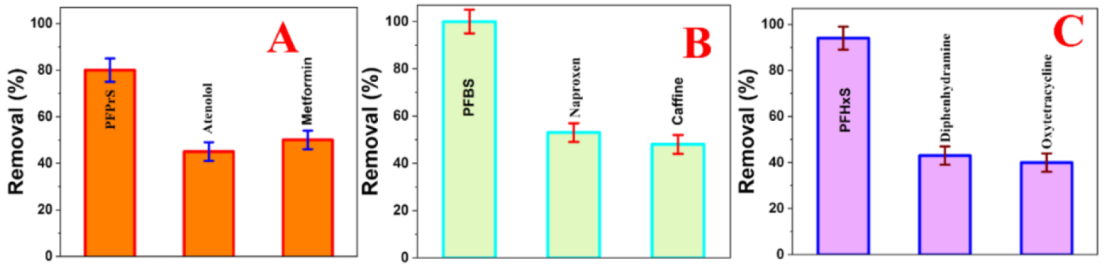

Figure 4. (A) Removal efficiency for ultrashort-chain PFPrS (1 μg/L), atenolol (1 μg/L), and metformin (1 μg/L) from drinking water using the nanoadsorbent (1 mg/L). (B) Removal efficiency for short-chain PFBS (1 μg/L), aproxen (1 μg/L), and caffeine (1 μg/L) from drinking water using the nanoadsorbent (1 mg/L). (C) Removal efficiency for short-chain PFHxS (1 μg/L), diphenhydramine (1 μg/L), and oxytetracycline (1 μg/L) from drinking water using the nanoadsorbent (1 mg/L).

The synthesis details are reported in the Supporting Information. PFBS separation data indicate that the efficiency for PFPrS removal is in the following order: NFBS-PEI-attached nanoadsorbent (q_m ~ 187 mg g^{-1}) > F-PEG-CH_2COOH-attached magnetic nanoadsorbent without PEI (q_m ~ 144 mg g^{-1}) > PEI-attached nanoadsorbent (q_m ~ 119 mg g^{-1}) > carboxylic acid-attached nanoadsorbent (q_m ~ 52 mg g^{-1}), which demonstrate that cooperative hydrophobic, fluorophilic, and electrostatic interactions are essential for highly efficient removal of emerging PFBS.

Understanding the Role of Cooperative Interactions in Long-, Short-, and Ultrashort-Chain PFAS Removal. Next, to determine comparative removal kinetics for long-, short-, and ultrashort-chain PFAS using the NFBS and PEI-attached magnetic nanoadsorbent, we have performed the capture and separation experiment for legacy PFAS like PFNA.

As reported in Figure 3F, the capture and removal efficiency for legacy PFNA is ~100% when the NFBS and PEI-conjugated magnetic nanoadsorbent has been used. On the other hand, as reported in Figure 3A, the capture and removal for short-chain PFBS is ~100% when the NFBS and PEI-conjugated magnetic nanoadsorbent has been used. Since PFNA has a much longer carbon chain than PFBS, one can expect stronger hydrophobic interactions for PFNA in comparison to PFBS. As reported in Figure 3F, the capture and removal efficiency for legacy PFNA is ~100% after 30 min. As reported in Table 1, the maximum capacity of PFBS adsorption by the NFBS and PEI-conjugated magnetic nanoadsorbent at equilibrium (q_m) is ~234 mg g^{-1}, which is comparable with the maximum capacity of PFNA adsorption by the NFBS and PEI-conjugated magnetic nanoadsorbent at equilibrium (q_m) being ~246 mg g^{-1}. All the above data clearly indicate that fluorophilic and electrostatic interactions play a very important role in the observed high capacity PFBS adsorption by the NFBS and PEI-conjugated magnetic nanoadsorbent. Similarly, as reported in Table 1, the maximum capacity of PFPrS adsorption by NFBS and PEI-conjugated magnetic nanoadsorbents at equilibrium (q_m) is ~186 mg g^{-1} and the maximum capacity of TFA adsorption by NFBS and PEI-conjugated magnetic nanoadsorbents at equilibrium (q_m) is ~170 mg g^{-1}.

The observed high removal capacity for ultra short-chain PFAS by NFBS and PEI-conjugated magnetic nanoadsorbents indicates that fluorophilic and electrostatic interactions play a very important role for the capturing of ultrashort-chain PFAS.

Demonstrating Selectivity of PFAS Capturing against Pharmaceutical Pollutants Using NFBS and PEI-Conjugated Multifunctional Magnetic Nanoadsorbents. It is now well documented that environmental pharmaceutical pollutants such as atenolol (β-blocker), metformin (anti-hyperglycemic), naproxen (anti-inflammatory), caffeine (stimulant and lifestyle compound), diphenhydramine (anti-histamine) and oxytetracycline (antimicrobial) has deleterious effects on human health and ecosystems.[40−45] To understand selectivity for capturing PFAS using NFBS and PEI-conjugated multifunctional magnetic nanoadsorbents, we have performed capture of different pharmaceutical, industrial, and flame-retardant pollutants using magnetic nanoadsorbents.

For this experiment, each of the contaminated samples was prepared by spiking the drinking water with 1 μg/L of PFAS or pharmaceutical, industrial, and flame-retardant pollutants individually. Figure 4B shows the removal efficiency for emerging PFBS, naproxen, and caffeine from drinking water. As reported in Figure 4B, although the removal efficiency for short-chain PFBS is ~100%, the removal efficiency for naproxen is ~36% and for the caffeine it is ~28%, which is due to the absence of −C-F bonds in naproxen and caffeine. As a result, they cannot participate in fluorophilic molecular interactions with a magnetic nanoadsorbent. Similarly, Figure 4C shows that the removal efficiency for emerging short-chain PFHxS is much higher than diphenhydramine and oxytetracycline, from drinking water. All the reported data clearly indicate that cooperative hydrophobic, fluorophilic, and electrostatic interactions are very important for high efficiency capturing of ultrashort- and short-chain PFAS.

On the other hand, as reported in Figure 4A, although the removal efficiency for ultrashort-chain PFPrS is much higher than the removal efficiency for atenolol and metformin. The observed low removal efficiency for pharmaceutical pollutants is due to the absence of −C-F bonds in atenolol or metformin, and thus, the fluorophilic interactions between nanoadsorbent and pharmaceutical pollutants are lacking.

Capturing Ultrashort- and Short-Chain PFAS from Environmental Reservoir, River, Lake, and Tap Water Samples Using NFBS and PEI-Conjugated Multifunctional Magnetic Nanoadsorbents. Next, we have determined whether NFBS and PEI-conjugated magnetic nanoadsorbents can be used for the selective and simultaneous separation of short-chain PFAS like GenX, PFHxS, PFBS, and PFBA and ultrashort-chain PFAS like PFPrS and TFA from the environmental water samples. For this purpose, we have used water from the Ross *Barnett Reservoir*, tap water, Grenada lake water, and Mississippi River water samples that were spiked with 1 μg/L of short-chain PFAS like GenX, PFHxS, PFBS, PFBA and ultrashort-chain PFAS like PFPrS, TFA individually. Further, we studied samples spiked with two different PFAS for

https://doi.org/10.1021/acsomega.4c07159
ACS Omega 2024, 9, 49452−49462

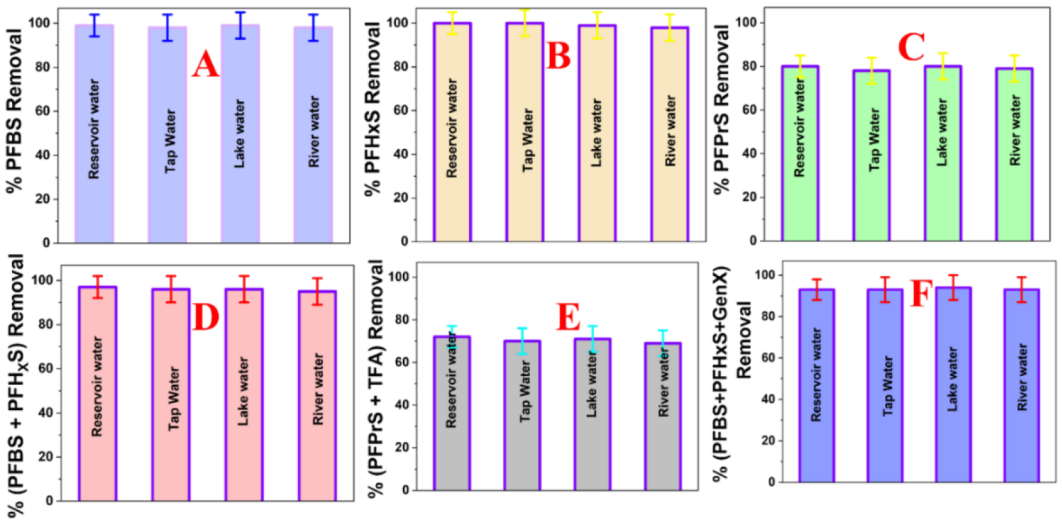

Figure 5. Removal efficiency of the nanoadsorbent (1 mg/L) for short- and ultrashort-chain PFAS samples prepared with water from different sources (Ross Barnett Reservoir water, tap water, Grenada lake water, and Mississippi River wa). (A) 1 μg/L emerging short-chain PFBS. (B) 1 μg/L short-chain PFHxS. (C) 1 μg/L ultrashort-chain PFPrS. (D) Mixture of 0.5 μg/L each of the short-chain PFBS and PFHxS. (E) Mixture of 0.5 μg/L of each of the ultrashort-chain PFPrS and TFA. (F) Mixture of 0.33 μg/L of each of the emerging PFBS, PFHxS, and GenX.

separation experiments, and those samples were spiked with 0.5 μg/L of each PFAS. We also explored water samples that were spiked with three different PFAS (0.33 μg/L of each PFAS).

Since the pH of the environmental samples varied for different sources, we have determined how the capture efficiency varies with the pH of water. The environmental samples we have used are from the Mississippi Bernett reservoir water (pH = 8.2), Grenada Lake water (pH = 6.7), Jackson tap water (pH = 7.5), and Mississippi River water (pH = 7.9), where pH varies between 6 and 9. As a result, we have determined how the maximum capacity of PFBS adsorption by NFBS and PEI-conjugated magnetic nanoadsorbent varies with the pH of water. Figure 3I shows pH dependent PFBS removal efficiency using NFBS and PEI-conjugated magnetic nanoadsorbent, which indicates that the q_m values vary from 234 mg g^{-1} to 222 mg $g^{-1,}$ as the pH varies from 6 to 9. Since the q_m value variation is small for PFOA as the pH changes from 6 to 9, we can neglect the pH variation effect for the removal efficiency from environmental samples of the Ross Barnett Reservoir water, tap water, Grenada lake water, and Mississippi River water samples.

As shown in Figure 5A, the NFBS and PEI-conjugated magnetic nanoadsorbent have the capability to remove ~98% of short-chain PFBS from water taken from different sources. Since all the environmental samples from Ross Barnett Reservoir water, Grenada lake water, and the Mississippi River water may contain different organic compounds, and heavy metals[45] our reported data indicates that NFBS and PEI-conjugated magnetic nanoadsorbent can be used for selective PFBS capture. As shown in Figure 5B, NFBS and PEI-conjugated magnetic nanoadsorbent has capability to remove ~96% of short-chain PFHxS from Ross Barnett Reservoir water, tap water, Grenada lake water, and Mississippi River water samples. Similarly, as reported in Figure 5C, NFBS and PEI-conjugated magnetic nanoadsorbent have the capability to remove ~78% of ultrashort-chain PFPrS from environmental water samples. This data shows the potential of multifunctional magnetic adsorbent materials for the removal of individual short-chain and legacy PFAS at environmentally relevant conditions. As reported in Figure 5D, the NFBS and PEI-conjugated magnetic nanoadsorbent has the capability to remove ~96% of short-chain PFBS and PFHxS simultaneously from the studied water samples. Similarly, as reported in Figure 5E, the NFBS and PEI-conjugated magnetic nanoadsorbent has the capability to remove ~70% of ultrashort-chain PFPrS and TFA simultaneously from environmental water samples. Further, Figure 5F shows that our developed magnetic nanoadsorbent has the capability to remove ~96% of short-chain PFBS, GenX, and PFHxS simultaneously from environmental water. This demonstrates that NFBS and PEI-conjugated magnetic nanoadsorbent can efficiently capture two PFAS simultaneously with high affinity even in the presence of other organic and inorganic contaminants.

Next to determine the reusability of the nanoadsorbents, we have performed PFAS separation experiments for different cycles using PFBS, PFHxS, GenX and PFBA infected Ross *Barnett Reservoir water*.Figure S7in theSupporting Information shows how the removal efficiency of nanoadsorbent for PFAS samples containing the mixture of 0.25 μg/L of each of the short-chain PFBS, PFHxS, GenX, and PFBA varies for different cycles. Reported data shows the removal efficiency decreases after 3 cycles, which can be due to the fact that the amount of fluorophilic and electrostatic interaction sites decreases as the number of cycles increases.

CONCLUSIONS

In conclusion, our findings reveal that cooperative hydrophobic, fluorophilic, and electrostatic interactions are very important for maximizing the removal capacity and selectivity for high efficiency capture of ultrashort and short-chain PFAS. Moreover, experimental data demonstrated that NFBS and PEI conjugated magnetic nanoadsorbents can be used for highly effective removal of short-chain PFAS like PFBS (~99%), PFHxS (~94%) and GenX (~92%) from contaminated drinking water within 30 min. We have also shown that magnetic nanoadsorbents have the capacity for efficient removal of ultrashort-chain PFAS like PFOrS (~80%) and TFA (~70%) from contaminated water within 30 min. Moreover, the reported data demonstrate the potential of

https://doi.org/10.1021/acsomega.4c07159
ACS Omega 2024, 9, 49452−49462

multifunctional magnetic adsorbent materials for the removal of ultrashort- and short-chain PFAS at environmentally relevant conditions from Ross Barnett Reservoir water, tap water, Grenada lake water, Mississippi River water samples. Although this work shows nanoadsorbents have the capability for real life applications, we are in an early stage for engineering the design of the magnetic nanoadsorbents. Future work will focus on optimizing the design for the complete removal of all different types of PFAS simultaneously from real water matrices.

■ ASSOCIATED CONTENT

Supporting Information

The Supporting Information is available free of charge at https://pubs.acs.org/doi/10.1021/acsomega.4c07159.

Detailed design and characterization of different magnetic nanoadsorbents and other experimental details are available as Supporting Information (PDF)

■ AUTHOR INFORMATION

Corresponding Author

Paresh Chandra Ray − *Department of Chemistry and Biochemistry, Jackson State University, Jackson, Mississippi 39217, United States;* orcid.org/0000-0001-5398-9930; Email: paresh.c.ray@jsums.edu; Fax: +16019793674

Authors

Avijit Pramanik − *Department of Chemistry and Biochemistry, Jackson State University, Jackson, Mississippi 39217, United States;* orcid.org/0000-0002-4623-2099

Olorunsola Praise Kolawole − *Department of Chemistry and Biochemistry, Jackson State University, Jackson, Mississippi 39217, United States*

Sanchita Kundu − *Department of Chemistry and Biochemistry, Jackson State University, Jackson, Mississippi 39217, United States;* orcid.org/0000-0002-9843-0476

Kaelin Gates − *Department of Chemistry and Biochemistry, Jackson State University, Jackson, Mississippi 39217, United States*

Shivangee Rai − *Department of Chemistry and Biochemistry, Jackson State University, Jackson, Mississippi 39217, United States*

Manoj K. Shukla − *US Army Engineer Research and Development Center, Vicksburg, Mississippi 39180-6199, United States;* orcid.org/0000-0002-7560-1172

Complete contact information is available at: https://pubs.acs.org/10.1021/acsomega.4c07159

Notes

The authors declare no competing financial interest.

■ ACKNOWLEDGMENTS

The use of trade, product, or firm named in this report is for descriptive purposes only and does not imply endorsement by the U.S. Government. The tests described and the resulting data presented herein, unless otherwise noted, were obtained from research conducted under the Environmental Quality Technology Program of the United States Army Corps of Engineers and the Environmental Security Technology Certification Program of the Department of Defense by the USAERDC. Permission was granted by the Chief of Engineers to publish this information. The findings of this report are not to be construed as an official Department of the Army position unless so designated by other authorized documents. Dr. Ray thanks the US Army Engineer Research and Development Center (ERDC), grant number W912HZ-23-2-0006, for their generous funding. Dr. Ray also thanks NSF-RISE grant no. EES-2219522 and NSF-PREM grant no. DMR-1826886 for their generous funding for the scholarship of graduate students.

■ REFERENCES

(1) United States Environmental Protection Agency. *Technical Fact Sheet: Drinking Water Health Advisories for Four PFAS (PFOA, PFOS, GenX Chemicals and PFBS)*. https://www.epa.gov/system/files/documents/2022-06/drinking-water-ha-pfas-factsheet-water-system.pdf (Accessed July 28, 2024).

(2) Lim, X. Can the World Leave 'Forever Chemicals' Behind? *Nature* **2023**, *620*, 24−27.

(3) Zheng, G.; Eick, S. M.; Salamova, A. Elevated Levels of Ultrashort- and Short-Chain Perfluoroalkyl Acids in US Homes and People. *Environ. Sci. Technol.* **2023**, *57* (42), 15782−15793.

(4) Neuwald, I. J.; Hübner, D.; Wiegand, H. L.; Valkov, V.; Borchers, U.; Nödler, K.; Scheurer, M.; Hale, S. E.; Arp, H. P. H.; Zahn, D. Ultra-Short-Chain PFASs in the Sources of German Drinking Water: Prevalent, Overlooked, Difficult to Remove, and Unregulated. *Environ. Sci. Technol.* **2022**, *56* (10), 6380−6390.

(5) Evich, M. G.; Davis, M. J. B.; McCord, J. P.; Acrey, B.; Awkerman, J. A.; Knappe, D. R. U.; Lindstrom, A. B.; Speth, T. F.; Tebes-Stevens, C.; Strynar, M. J.; Wang, Z.; Weber, E. J.; Henderson, W. M.; Washington, J. W. Per- and polyfluoroalkyl substances in the environment. *Science* **2022**, *375*, No. eabg9065.

(6) Joudan, S.; Gauthier, J.; Mabury, S. A.; Young, C. J. Aqueous Leaching of Ultrashort-Chain PFAS from (Fluoro) polymers: Targeted and Nontargeted Analysis. *Environmental Science & Technology Letters* **2024**, *11* (3), 237−242.

(7) Chen, Z.; Lu, Y. L.; Wang, L.; Xu, J.; Zhang, J.; Xu, X.; Cheng, P.; Yang, S.; Shi, W. Efficient Recognition and Removal of Persistent Organic Pollutants by a Bifunctional Molecular Material. *J. Am. Chem. Soc.* **2023**, *145*, 260−267.

(8) Jacob, P.; Helbling, D. E. Rapid and Simultaneous Quantification of Short- and Ultrashort-Chain Perfluoroalkyl Substances in Water and Wastewater. *ACS ES&T Water* **2023**, *3*, 118−128.

(9) Huang, J.; Shi, Y.; Huang, G.-Z.; Huang, S.; Zheng, J.; Xu, J.; Zhu, F.; Ouyang, G. Facile Synthesis of a Fluorinated-Squaramide Covalent Organic Framework for the Highly Efficient and Broad-Spectrum Removal of Per- and Polyfluoroalkyl Pollutants. *Angew. Chem., Int. Ed.* **2022**, *61* (31), No. e202206749.

(10) Liu, X.; Zhu, C.; Yin, J.; Li, J.; Zhang, Z.; Li, J.; Shui, F.; You, Z.; Shi, Z.; Li, B. Installation of synergistic binding sites onto porous organic polymers for efficient removal of perfluorooctanoic acid. *Nat. Commun.* **2022**, *13* (1), 2132−2132.

(11) Liang, R. R.; Xu, S.; Han, Z.; Yang, Y.; Wang, K. Y.; Huang, Z.; Rushlow, J.; Cai, P.; Samorìm, P.; Zhou, H.-C. Exceptionally High Perfluorooctanoic Acid Uptake in Water by a Zirconium-Based Metal−Organic Framework through Synergistic Chemical and Physical Adsorption. *J. Am. Chem. Soc.* **2024**, *146* (14), 9811−9818.

(12) Ateia, M.; Alsbaiee, A.; Karanfil, T.; Dichtel, W. Efficient PFAS Removal by Amine-Functionalized Sorbents: Critical Review of Current Literature. *Environ. Sci. Technol. Lett.* **2019**, *6* (12), 688−695.

(13) Kumarasamy, E.; Manning, I. M.; Collins, L. B.; Coronell, O.; Leibfarth, F. A. Ionic Fluorogels for Remediation of Per- and Polyfluorinated Alkyl Substances from Water. *ACS Cent. Sci.* **2020**, *6*, 487−492.

(14) Román Santiago, A.; Yin, S.; Elbert, J.; Lee, J.; Shukla, D.; Su, X. Imparting Selective Fluorophilic Interactions in Redox Copolymers for the Electrochemically Mediated Capture of Short-Chain Perfluoroalkyl Substances. *J. Am. Chem. Soc.* **2023**, *145* (17), 9508−9519.

(15) Tan, X.; Zhong, J.; Fu, C.; Dang, H.; Han, Y.; Král, P.; Guo, J.; Yuan, Z.; Peng, H.; Zhang, C.; Whittaker, A. K. Amphiphilic

https://doi.org/10.1021/acsomega.4c07159
ACS Omega 2024, 9, 49452−49462

Perfluoropolyether Copolymers for the Effective Removal of Polyfluoroalkyl Substances from Aqueous Environments. *Macromolecules* **2021**, *54*, 3447−3457.
(16) Shetty, D.; Jahović, I.; Skorjanc, T.; Erkal, T. S.; Ali, L.; Raya, J.; Asfari, Z.; Olson, M. A.; Kirmizialtin, S.; Yazaydin, A. O.; Trabolsi, A. Rapid and Efficient Removal of Perfluorooctanoic Acid from Water with Fluorine-Rich Calixarene-Based Porous Polymers. *ACS Appl. Mater. Interfaces* **2020**, *12*, 43160−43166.
(17) Tan, X.; Dewapriya, P.; Prasad, P.; Chang, Y.; Huang, X.; Wang, Y.; Gong, X.; Hopkins, T. E.; Fu, C.; Thomas, K. V.; Peng, H.; Whittaker, A. K.; Zhang, C. Efficient Removal of Perfluorinated Chemicals from Contaminated Water Sources Using Magnetic Fluorinated Polymer Sorbents. *Angew. Chem., Int. Ed.* **2022**, *61*, No. e202213071.
(18) Manning, I. M.; Chew, N. G. P.; Macdonald, H. P.; Miller, K. E.; Strynar, M. J.; Coronell, O.; Leibfarth, F. A. Hydrolytically Stable Ionic Fluorogels for High-Performance Remediation of Per- and Polyfluoroalkyl Substances (PFAS) from Natural Water. *Angew. Chem., Int. Ed.* **2022**, *61*, No. e202208150.
(19) Ji, W.; Xiao, L.; Ling, Y.; Ching, C.; Matsumoto, M.; Bisbey, R. P.; Helbling, D. E.; Dichtel, W. R. Removal of GenX and Perfluorinated Alkyl Substances from Water by Amine-Functionalized Covalent Organic Frameworks. *J. Am. Chem. Soc.* **2018**, *140*, 12677−12681.
(20) Pramanik, A.; Kolawole, O. P.; Gates, K.; Kundu, S.; Shukla, M. K.; Moser, R. D.; Ucak-Astarlioglu, M.; Al-Ostaz, A.; Ray, P. C. 2D Fluorinated Graphene Oxide (FGO)-Polyethyleneimine (PEI) Based 3D Porous Nanoplatform for Effective Removal of Forever Toxic Chemicals, Pharmaceutical Toxins, and Waterborne Pathogens from Environmental Water Samples. *ACS Omega* **2023**, *8* (47), 44942−44954.
(21) Mantripragada, S.; Obare, S. O.; Zhang, L. Addressing Short-Chain PFAS Contamination in Water with Nanofibrous Adsorbent/Filter Material from Electrospinning. *Acc. Chem. Res.* **2023**, *56*, 1271−1278.
(22) Choudhary, A.; Bedrov, D. Interaction of Short-Chain PFAS with Polycationic Gels: How Much Fluorination is Necessary for Efficient Adsorption? *ACS Macro Lett.* **2022**, *11* (9), 1123−1128.
(23) Mantripragada, S.; Deng, D.; Zhang, L. Remediation of GenX from Water by Amidoxime Surface-Functionalized Electrospun Polyacrylonitrile Nanofibrous Adsorbent. *Chemosphere* **2021**, *283*, No. 131235.
(24) Choudhary, A.; Dong, D.; Tsianou, M.; Alexandridis, P.; Bedrov, D. Adsorption Mechanism of Perfluorooctanoate on Cyclodextrin-Based Polymers: Probing the Synergy of Electrostatic and Hydrophobic Interactions with Molecular Dynamics Simulations. *ACS Mater. Lett.* **2022**, *4* (5), 853−859.
(25) Lei, X.; Lian, Q.; Zhang, X.; Wang, T.; Gee, M.; Holmes, W.; Jin, S.; Ponnusamy, S. K.; Gang, D. S.; Zappi, M. E. Removal of perfluorooctanoic acid via polyethyleneimine modified graphene oxide: Effects of water matrices and understanding mechanisms. *Chemosphere* **2022**, *308*, No. 136379.
(26) Xiao, L.; Ling, Y.; Alsbaiee, A.; Li, C.; Helbling, D. E.; Dichtel, W. R. β-Cyclodextrin Polymer Network Sequesters Perfluorooctanoic Acid at Environmentally Relevant Concentrations. *J. Am. Chem. Soc.* **2017**, *139*, 7689−7692.
(27) Ateia, M.; Attia, M. F.; Maroli, A.; Tharayil, N.; Alexis, F.; Whitehead, D. C.; Karanfil, T. Rapid Removal of Poly- and Perfluorinated Alkyl Substances by Poly(Ethylenimine)-Functionalized Cellulose Microcrystals at Environmentally Relevant Conditions. *Environ. Sci. Technol. Lett.* **2018**, *5*, 764−769.
(28) Hassan, M.; Du, J.; Liu, Y.; Naidu, R.; Zhnag, J.; Ahsan, M. A.; Qi, F. Magnetic biochar for removal of perfluorooctane sulphonate (PFOS): Interfacial interaction and adsorption mechanism. *Environ. Technol. Innovation* **2022**, *28*, No. 102593.
(29) Yang, A.; Ching, C.; Easler, M.; Helbling, D. E.; Dichtel, W. R. Cyclodextrin Polymers with Nitrogen-Containing Tripodal Crosslinkers for Efficient PFAS Adsorption. *ACS Mater. Lett.* **2020**, *2* (9), 1240−1245.
(30) Zhang, C.; Yan, K.; Fu, C.; Peng, H.; Hawker, C. J.; Whittaker, A. K. Biological Utility of Fluorinated Compounds: from Materials Design to Molecular Imaging, Therapeutics and Environmental Remediation. *Chem. Rev.* **2022**, *122*, 167−208.
(31) Meng, P.; Fang, X.; Maimaiti, A.; Yu, G.; Deng, S. Efficient removal of perfluorinated compounds from water using a regenerable magnetic activated carbon. *Chemosphere* **2019**, *224*, 187−194.
(32) Parker, B. A.; Knappe, D. R. U.; Titaley, I. A.; Wanzek, T. A.; Field, J. A. Tools for Understanding and Predicting the Affinity of Per- and Polyfluoroalkyl Substances for Anion-Exchange Sorbents. *Environ. Sci. Technol.* **2022**, *56* (22), 15470−15477.
(33) Wang, R.; Lin, Z.-W.; Klemes, M. J.; Ateia, M.; Trang, B.; Wang, J.; Ching, C.; Helbling, D. E.; Dichtel, W. R. A Tunable Porous β-Cyclodextrin Polymer Platform to Understand and Improve Anionic PFAS Removal. *ACS Cent. Sci.* **2022**, *8* (5), 663−66.
(34) Lin, Z.-W.; Shapiro, E. F.; Barajas-Rodriguez, F. J.; Gaisin, A.; Ateia, M.; Currie, J.; Helbling, D. E.; Gwinn, R.; Packman, A. I.; Dichtel, W. R. Trace organic contaminant removal from municipal wastewater by styrenic β-cyclodextrin polymers. *Environ. Sci. Technol.* **2023**, *57* (48), 19624−19636.
(35) Pramanik, A.; Mayer, J.; Sinha, S. S.; Sharma, P. C.; Patibandla, S.; Gao, Ye; Corby, L. R.; Bates, J. T.; Bierdeman, M. A.; Tandon, R.; Seshadri, R.; Ray, P. C. Human ACE2 Peptide-Attached Plasmonic-Magnetic Heterostructure for Magnetic Separation, Surface Enhanced Raman Spectroscopy Identification, and Inhibition of Different Variants of SARS-CoV-2 Infections. *ACS Appl. Bio Mater.* **2022**, *5* (9), 4454−4464.
(36) Pramanik, A.; Vangara, A.; Nellore, B. P. V.; Sinha, S. S.; Chavva, S. R.; Jones, S.; Ray, P. C. Development of Multifunctional Fluorescent-Magnetic Nanoprobes for Selective Capturing and Multicolor Imaging of Heterogeneous Circulating Tumor Cells. *ACS Appl. Mater. Interfaces* **2016**, *8*, 15076−15085.
(37) Laurent, S.; Forge, D.; Port, M.; Roch, A.; Robic, C.; Vander Elst, L.; Muller, R. N. Magnetic Iron Oxide Nanoparticles: Synthesis, Stabilization, Vectorization, Physicochemical Characterizations, and Biological Applications. *Chem. Rev.* **2008**, *108*, 2064−2110.
(38) Pramanik, A.; Kundu, S.; Gates, K.; Kumar, A.; Kolawole, O. P.; Talukdar, A.; Iftekhar, R.; Corby, L. R.; Ray, P. C. Multi-Color-Emissive Magneto-Luminescent Nanoadsorbentss for Targeted Identification of Heterogeneous Exosomes Associated with Lung Cancer Metastasis. *ACS Applied Bio Materials* **2023**, *6*, 2446−2458.
(39) Shingte, S. D.; Phakatkar, A. H.; McKiernan, E.; Nigoghossian, K.; Ferguson, S.; Shahbazian-Yassar, R.; Brougham, D. F. Correlating Magnetic Hyperthermia and Magnetic Resonance Imaging Contrast Performance of Cubic Iron Oxide Nanoparticles with Crystal Structural Integrity. *Chem. Mater.* **2022**, *34*, 10801−10810.
(40) Zhang, W.; Xu, H.; Xie, F.; Ma, X.; Niu, B.; Chen, M.; Zhang, H.; Zhang, Y.; Long, D. General synthesis of ultrafine metal oxide/reduced graphene oxide nanocomposites for ultrahigh-flux nanofiltration membrane. *Nat. Commun.* **2022**, *13* (1), 471.
(41) Ruan, T.; Li, P.; Wang, H.; Li, T.; Jiang, G. Identification and Prioritization of Environmental Organic Pollutants: From an Analytical and Toxicological Perspective. *Chem. Rev.* **2023**, *123* (17), 10584−10640.
(42) Schwarzenbach, R. P.; Egli, T.; Hofstetter, T. B.; von Gunten, U.; Wehrli, B. Global Water Pollution and Human Health. *Annu. Rev. Environ. Resour.* **2010**, *35*, 109−136.
(43) Chen, Y.; Jiang, C.; Wang, Y.; Song, R.; Tan, Y.; Yang, Y.; Zhang, Z. Sources, Environmental Fate, and Ecological Risks of Antibiotics in Sediments of Asia's Longest River: A Whole-Basin Investigation. *Environ. Sci. Technol.* **2022**, *56* (20), 14439−14451.
(44) Patel, M.; Kumar, R.; Kishor, K.; Mlsna, T.; Pittman, C. U., Jr; Mohan, D. Pharmaceuticals of Emerging Concern in Aquatic Systems: Chemistry, Occurrence, Effects, and Removal Methods. *Chem. Rev.* **2019**, *119*, 3510−3673.
(45) Santschi, P. H.; Presley, B. J.; Wade, T. L.; Garcia-Romero, B.; Baskaran, M. Historical contamination of PAHs, PCBs, DDTs, and heavy metals in Mississippi River Delta, Galveston Bay and Tampa Bay sediment cores. *Mar Environ. Res.* **2001**, *52*, 51−79.

https://doi.org/10.1021/acsomega.4c07159
ACS Omega 2024, 9, 49452−49462